



1 **A GIS-based three-dimensional landslide generated waves height calculation**
2 **method**

3
4 Guo Yu¹, Mowen Xie^{1,*}, Lei Bu¹, Asim Farooq²

5 ¹ School of Civil and Resource Engineering, University of Science & Technology
6 Beijing, Beijing 100083, China

7 ²CECOS University, Peshawar Pakistan

8 * Corresponding author: Mowen Xie (mowenxie123@163.com)

9
10 **Abstract:** Combined with the spatial data processing capability of geographic
11 information systems (GIS), a three-dimensional (3D) landslide surge height calculation
12 method is proposed based on grid column units. First, the data related to the landslide
13 are rasterized to form grid columns, and a force analysis model of 3D landslides is
14 established. Combining the vertical strip method with Newton's laws of motion,
15 dynamic equilibrium equations are established to solve for the surge height. Moreover,
16 a 3D landslide surge height calculation expansion module is developed in the GIS
17 environment, and the results are compared with those of the two-dimensional Pan
18 Jiazheng method. Comparisons show that the maximum surge height obtained by the
19 proposed method is 24.6% larger than that based on the Pan Jiazheng method.
20 Compared with the traditional two-dimensional method, the 3D method proposed in
21 this paper better represents the actual spatial state of the landslide and is more suitable
22 for risk assessment.

23 **Key words:** landslide; waves height; grid column; GIS

24 **1. Introduction**

25 When a reservoir bank landslide body slides into the water, it will cause a waves
26 that can not only endanger the safety of passing ships and surrounding buildings but
27 also threaten the safety of the dam. Therefore, calculating the waves height is important
28 for evaluating the risks of landslides (Xu and Zhou, 2015).

29 The methods of calculating the landslide generated waves height can mainly be
30 divided into analytical method (Noda, 1970; Pan, 1980; Huang et al., 2012; Miao et al., 2011;
31 Di et al., 2008), numerical simulation method (Silvia and Marco, 2011; Montagna et al.,
32 2011), and physical modelling method (Ataie-Ashtiani and Nik-Khah, 2008; Cui and Zhu,
33 2011). Analytical method is widely used in engineering applications because of its



34 simple modelling processes, which has few requirements for engineers and high
35 precision.

36 The analytical method originated from Node (1970). Node proposed the waves
37 height calculation method on the basis of hydraulics. Since then, many scholars have
38 conducted more in-depth research. For example, Academician Pan Jiazheng of China
39 divided the landslide body into many two-dimensional (2D) vertical strips and
40 calculated the waves height by considering the horizontal and vertical movement of the
41 landslide. This method is called the Pan Jiazheng method (Pan, 1980). Huang et al. (2012)
42 improved the Pan Jiazheng method by considering the resistance of water and the
43 change in the friction coefficient. Miao et al. (2011) proposed a sliding block model
44 based on the 2D vertical strip method to predict the maximum waves height. The
45 American Civil Engineering Society recommends a prediction method of the waves
46 height (Di et al., 2008) that assumes the landslide results in the particle motion with a
47 centre of gravity, and Newton's law of motion is used to calculate the waves height.

48 The above methods are all 2D analysis methods. In the vertical strip method, the
49 calculation results will differ with the selection of the 2D section. The 2D analysis
50 methods cannot effectively simulate the actual spatial state of three-dimensional (3D)
51 landslide. Hu (Hu, 1995) proposed that the value obtained by 2D analysis method is
52 approximately 70% of the value based on 3D analysis method. To date, analytical
53 method based on the 3D landslide body model has not been studied by scholars.

54 Geographic information systems (GIS) is widely used in geotechnical engineering.
55 The most notable feature of GIS is that they can transform vector data into grid data
56 sets based on a grid column unit model (Xie et al., 2006a). Because of the high 3D spatial
57 data processing capability of GIS, many scholars have added geotechnical professional
58 models to their respective systems. For example, our research team established a 3D
59 limit equilibrium method based on GIS, and developed a slope stability analysis module
60 called 3Dslope (Xie et al., 2003a; 2003b; 2006b). Jia et al. (2015) proposed a slope stability
61 analysis method by coupling a rainfall infiltration model and 3D limit equilibrium
62 method within the GIS environment. Mergili (2014) combined GRASS GIS and the 3D
63 Hovland model to implement a 3D slope stability model capable of considering shallow
64 and deep-seated slope failures. Therefore, to develop a waves height calculation module
65 in GIS, it is necessary to first establish a force analysis model of the 3D landslide in
66 GIS.

67 Based on the spatial data processing capability of GIS, this paper applies the grid

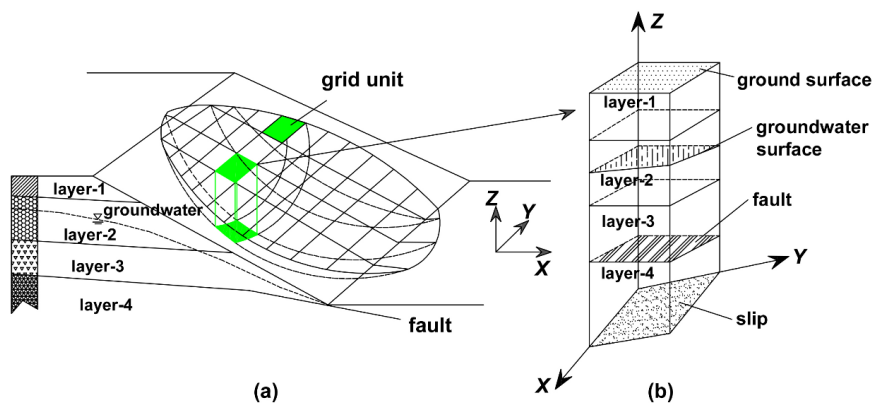


68 column unit model to establish a 3D landslide model, and proposes a method for
69 calculating the waves height. Compared with 2D analysis methods, the 3D method
70 proposed in this paper better represents the actual spatial state of landslides.
71 Simultaneously, the resistance of the water is considered to improve the accuracy of the
72 calculation result. To make the calculation more convenient, an expansion module is
73 developed to calculate the waves height in GIS, and the feasibility of the module is
74 verified by a case study.

75 2. GIS-based method of calculating the waves height

76 2.1. Grid column unit model

77 For a slope, the representation of data is mainly in the form of vectors. These data
78 include but are not limited to slip surface, strata, groundwater, fault, slip, and other
79 types of data. These vector data layers can be converted to raster data layers using the
80 spatial analysis capabilities of GIS to form a grid data set. The grid data structure
81 consists of rectangular units. Each rectangular unit has a corresponding row and column
82 number and is assigned an attribute value that represents the grid unit (Xie et al., 2004).
83 Therefore, the slope can be divided into square columns based on the grid units to form
84 a grid column unit model, as shown in Fig. 1.



85
86 **Fig. 1.** Grid column unit model ((a) 3D view of landslide, (b) 3D view of one column).

87 2.1. Force analysis

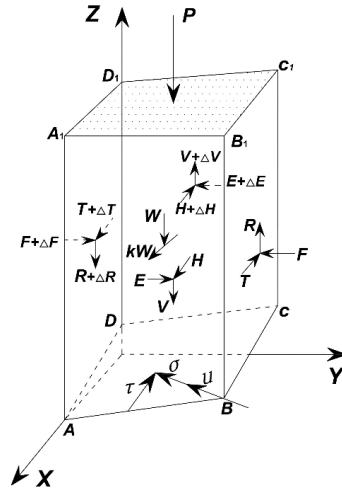
88 First, we arbitrarily selected a grid column in a 3D landslide body, as shown in
89 Fig. 2. We can specify the forces acting on the grid column as follows.

90 (1) The weight of one grid column is W ; the direction is the Z -axis; and the weight
91 acts at the centroid of the grid column.

92 (2) The resultant horizontal seismic force is kW , where k is the “seismic



93 coefficient"; the direction of kW is the sliding direction of the landslide; and the
 94 resultant horizontal force acts at the centroid of the grid column.



95

Fig. 2. Force analysis of one grid column.

96

97 (3) The external loads on the ground surface are represented by P ; the direction of
 98 P is the Z -axis, and these external loads act at the centre of the top of the grid column.

99 (4) The normal and shear stresses on the slip surface are represented by σ and τ ,
 100 respectively. The normal stress is perpendicular to the slip surface, and the shear stress
 101 is in the sliding direction of the landslide. The normal and shear stresses act at the
 102 centroid of the bottom of the grid column.

103 (5) The pore water pressure on the slip surface is u .

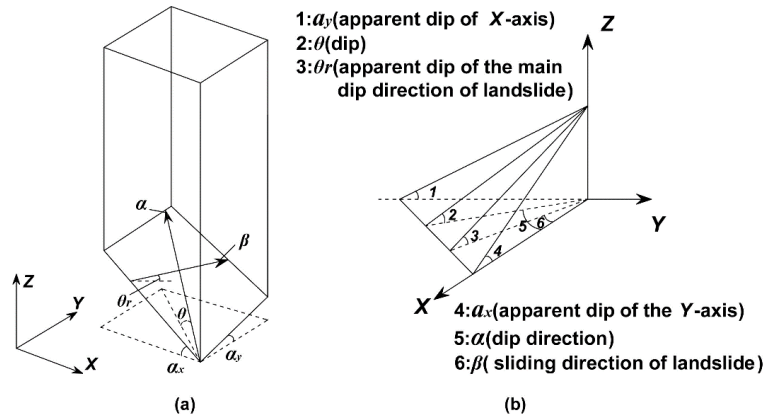
104 (6) The horizontal tangential forces on the left and right sides of a grid column are
 105 T and $T+\Delta T$, respectively; the vertical tangential forces on the left and right sides of a
 106 grid column are R and $R+\Delta R$, respectively; the normal forces on the left and right sides
 107 of a grid column are F and $F+\Delta F$, respectively; the horizontal tangential forces on the
 108 front and rear sides of a grid column are E and $E+\Delta E$, respectively; the vertical
 109 tangential forces on the front and rear sides of a grid column are V and $V+\Delta V$,
 110 respectively; and the normal forces on the front and rear sides of a grid column are H
 111 and $H+\Delta H$, respectively. For convenience, the resultant force between columns in the
 112 sliding direction of the landslide is defined as ΔD .

113 **2.3. The spatial relationships among parameters**

114 Fig. 3 shows the 3D spatial relationships among parameters on the slip surface. θ



115 is the dip of the grid column at the slip surface; α is the dip direction of the grid column
 116 at the slip surface; β is the sliding direction of the landslide; θ_r is the apparent dip of the
 117 main inclination direction of the landslide; α_x is the apparent dip of the X -axis; and α_y
 118 is the apparent dip of the Y -axis.



119

120 **Fig. 3.** 3D spatial relationships among parameters at the slip surface. ((a)
 121 and (b) are the spatial relationships for 3D views of one grid column and
 122 the coordinate system, respectively).

123 As shown in Fig. 3, the apparent dips of the X -axis and Y -axis are as follows.

$$124 \quad \tan \alpha_x = \cos \alpha \tan \theta, \quad \tan \alpha_y = \sin \alpha \tan \theta \quad (1)$$

125 The slip surface area of one grid column is calculated by

$$126 \quad A = \text{cellsize}^2 \left[\frac{\sqrt{(1 - \sin^2 \alpha_x \sin^2 \alpha_y)}}{\cos \alpha_x \cos \alpha_y} \right] \quad (2)$$

127 where *cellsize* represents the size of each grid column.

128 The apparent dip in the main inclination direction of the landslide is calculated as
 129 follows.

$$130 \quad \tan \theta_r = \tan \theta |\cos(\alpha - \beta)| \quad (3)$$

131 The weight W of the grid column is expressed as

$$132 \quad W = \text{cellsize}^2 \sum_{m=1}^n h_m r_m \quad (4)$$

133 where m is the number of strata, h_m is the height of each stratum, and r_m is the unit
 134 weight of each stratum. For the grid column units above the water, r_m is calculated from
 135 the natural unit weight. For grid column units under water, r_m is calculated from the



136 buoyant unit weight.

137 The pore water pressure is obtained as follows (Zhang, 2016).

$$138 \quad u = \frac{D}{\cos \theta} \quad (5)$$

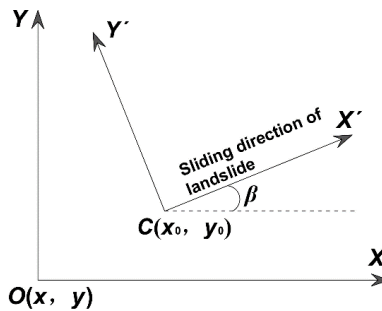
139 where D is the distance from the centre bottom of the grid column to the water surface.

140 When the sliding body enters the water, the resistance of the water is calculated as
 141 follows (Chow, 1979).

$$142 \quad G = \frac{1}{2} c_w \rho_f v^2 S \quad (6)$$

143 where G is the resultant force of the resistance of the water to the sliding body; c_w is the
 144 viscous resistance coefficient, which is 0.18; ρ_f is the buoyant density (g/m^3), taking the
 145 average of all stratum; v is the velocity of the landslide (m/s); and S is the surface area
 146 of the grid column in the water (m^2).

147 **2.4. Coordinate system conversion**



148

149

Fig. 4. Coordinate system conversion.

150 To facilitate subsequent calculations, the XOY coordinate system was converted to
 151 an $X'CY'$ coordinate system. The X' -axis direction was defined as the sliding direction
 152 of the landslide. The right-hand rule determined the positive directions of the Y' - and
 153 Z -axes. In addition, point O , i.e., the origin of the XOY coordinate system, was
 154 translated to point C in the $X'CY'$ coordinate system, as shown in Fig. 4. The
 155 transformation of the coordinates can be expressed as follows:

$$156 \quad \begin{Bmatrix} x' \\ y' \end{Bmatrix} = \begin{bmatrix} \cos(90^\circ - \beta) & \sin(90^\circ - \beta) \\ -\sin(90^\circ - \beta) & \cos(90^\circ - \beta) \end{bmatrix} \begin{Bmatrix} x - x_0 \\ y - y_0 \end{Bmatrix} \quad (7)$$

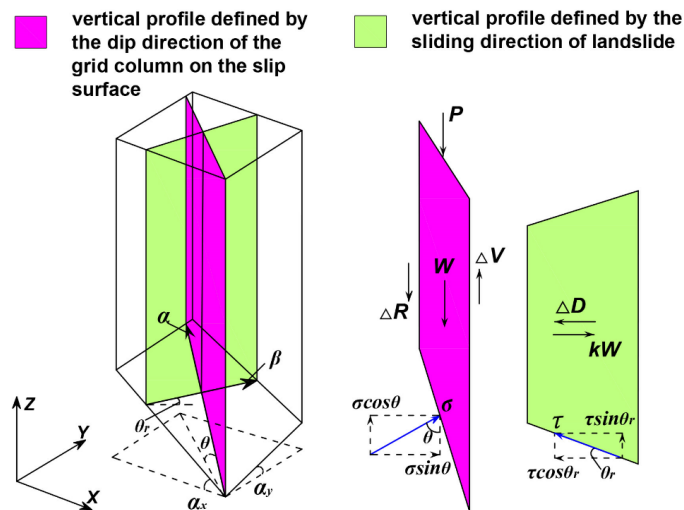
157 where x' and y' are the coordinate values of the centre bottom of each grid column
 158 in the $X'CY'$ coordinate system. x and y are the coordinate values of the centre
 159 bottom of each grid column in the XOY coordinate system; and x_0 and y_0 are the



160 coordinate values of point C in the XOY coordinate system.

161 **2.5. Dynamic equation based on grid column units**

162 We assume that all of the grid column units move continuously, do not separate in
 163 the macroscopic dimension and remain vertical after sliding, as also assumed by Pan
 164 Jiazheng (Pan, 1980). The force analysis of one grid column and the spatial relationships
 165 among parameters at the slip surface are shown in Fig. 2 and Fig. 3, respectively.



166

167 **Fig. 5.** Force analysis in the vertical direction and sliding direction of the landslide.

168 We arbitrarily selected a grid column unit (the grid column unit in row i and
 169 column j). According to Newton's laws of motion, dynamic equilibrium equations are
 170 established in the sliding direction of the landslide and the vertical direction. The force
 171 analyses in the sliding direction of the landslide and vertical direction are shown in
 172 Fig. 5.

173
$$A_{i,j} \tau_{i,j} \cos \theta_{r,i,j} - A_{i,j} \sigma_{i,j} \sin \theta_{i,j} \cos(\alpha_{i,j} - \beta) - kW_{i,j} + \Delta D_{i,j} - G_{i,j} = \frac{W_{i,j}}{g} a_x \quad (8)$$

174
$$A_{i,j} \tau_{i,j} \sin \theta_{r,i,j} + A_{i,j} \sigma_{i,j} \cos \theta_{i,j} - W_{i,j} - P_{i,j} + \Delta V_{i,j} - \Delta R_{i,j} = \frac{W_{i,j}}{g} a_{y_{i,j}} \quad (9)$$

175 where

176
$$\tau_{i,j} = c_{i,j} + (\sigma_{i,j} - u_{i,j}) \tan \varphi_{i,j} \quad (10)$$

177 where a_x and $a_{y_{i,j}}$ are the horizontal acceleration and vertical acceleration of the grid
 178 column, respectively; $\varphi_{i,j}$ is the effective friction angle of the grid column at the slip



179 surface; g is gravitational acceleration; $c_{i,j}$ is the effective cohesion of the grid column
 180 at the slip surface; and $G_{i,j}$ is the resistance of water to the grid column. For grid column
 181 units above water, $u_{i,j}$ is calculated by Eq. (5), and $W_{i,j}$ is calculated by taking the
 182 natural unit weight. For grid column units under water, $u_{i,j}$ is 0, and $W_{i,j}$ is calculated
 183 based on the buoyant unit weight.

184 According to this assumption, the horizontal acceleration a_x of each grid column
 185 unit is the same, and the vertical acceleration $a_{y_{i,j}}$ of each grid column unit varies. Pan
 186 Jiazheng suggested that (Pan, 1980) there is a certain proportional relationship between
 187 a_x and $a_{y_{i,j}}$, that is, $a_{y_{i,j}}/a_x = \tan \delta_{i,j}$. $\delta_{i,j}$ is the horizontal inclination angle of the line
 188 connecting the centre bottom of the grid column to the centre bottom of the next grid
 189 column in the sliding direction of the landslide. The effect of vertical tangential forces
 190 is ignored, namely, $\Delta V_{i,j} - \Delta R_{i,j} = 0$; therefore, Eq. (9) can be transformed as follows.

$$191 \quad A_{i,j} \tau_{i,j} \sin \theta_{r_{i,j}} + A_{i,j} \sigma_{i,j} \cos \theta_{i,j} - W_{i,j} - P_{i,j} = \frac{W_{i,j}}{g} a_x \tan \delta_{i,j} \quad (11)$$

192 The simultaneous Eqs. (10) and (11) can be obtained as follows.

$$193 \quad \sigma_{i,j} = \frac{A_{i,j} \sin \theta_{r_{i,j}} (u_{i,j} \tan \varphi_{i,j} - c_{i,j}) + W_{i,j} + P_{i,j} + \frac{W_{i,j}}{g} a_x \tan \delta_{i,j}}{A_{i,j} (\sin \theta_{r_{i,j}} \tan \varphi_{i,j} + \cos \theta_{i,j})} \quad (12)$$

194 For the entire sliding body, the forces between the grid columns are internal forces,
 195 that is, the resultant force is 0, yielding Eq. (13).

$$196 \quad \sum_I \sum_J \Delta D_{i,j} = 0 \quad (13)$$

197 By summing all the grid column units, the horizontal acceleration a_x can be
 198 determined by Eq. (8).

$$199 \quad a_x = \left[\sum_I \sum_J \frac{A_{i,j} \tau_{i,j} \cos \theta_{r_{i,j}} - A_{i,j} \sigma_{i,j} \sin \theta_{i,j} \cos(\alpha_{i,j} - \beta) - kW_{i,j} - G_{i,j}}{W_{i,j}} \right] g \quad (14)$$

200 Substituting Eqs. (10) and (12) into Eq. (14) yields the following equation.

$$201 \quad a_x = \left[\sum_I \sum_J \frac{B_{i,j} + E_{i,j} - F_{i,j} - (G_{i,j} \tan \delta_{i,j} H_{i,j} - kW_{i,j}) L_{i,j}}{W_{i,j} \tan \delta_{i,j} H_{i,j} Q_{i,j}} \right] g \quad (15)$$

202 where

$$203 \quad B_{i,j} = A_{i,j} \cos \theta_{r_{i,j}} (u_{i,j} c \tan \varphi_{i,j} - c_{i,j}^2) \quad (16)$$



204 $E_{i,j} = A_{i,j} \cos(\alpha_{i,j} - \beta) \sin \theta_{r_{i,j}} \sin \theta_{i,j} (u_{i,j} \tan \varphi_{i,j} - c_{i,j})$ (17)

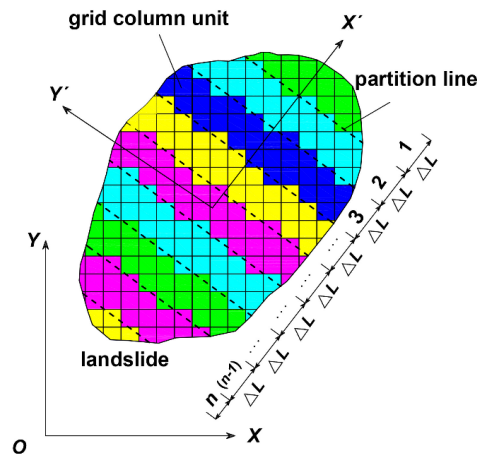
205 $F_{i,j} = [\cos \theta_{r_{i,j}} \tan \varphi_{i,j} - \sin \theta_{i,j} \cos(\alpha_{i,j} - \beta)] (W_{i,j} + P_{i,j})$ (18)

206 $L_{i,j} = c_{i,j} + \sin \theta_{r_{i,j}} \tan \varphi_{i,j}$ (19)

207 $H_{i,j} = \cos \theta_{r_{i,j}} \tan \varphi_{i,j} - \sin \theta_{i,j} \cos(\alpha_{i,j} - \beta)$ (20)

208 $Q_{i,j} = c_{i,j} + \sin \theta_{r_{i,j}} \tan \varphi_{i,j}$ (21)

209 **2.6. Calculation of the sliding velocity**



210
 211

Fig. 6. Rasterization and partitioning of landslides.

212 The steps in calculating the landslide sliding velocity are as follows.

213 (1) Using the spatial analysis capability of GIS, the landslide body is rasterized,
 214 and the size of the grid column unit (i, j) can be set to an arbitrary square. A partitioning
 215 line is drawn from the bottom to the top of the landslide every ΔL in the sliding direction
 216 of the landslide, and the resulting regions are numbered zone 1, zone 2, zone 3, ..., zone
 217 ($n-1$), zone n . Each partition includes a number of grid column units, and the length of
 218 zone n is less than or equal to ΔL , as shown in Fig. 6. For a grid column unit that is not
 219 completely contained within a partition, if the area within the partition is greater than
 220 half of the total area, the unit is divided into that partition; otherwise, the unit is divided
 221 into the next partition.

222 (2) For each grid column unit, the parameters required in Eq. (15) are calculated.

223 (3) t_0 is the starting point of when the landslide body begins to slide, and $t_0=0$.
 224 When the landslide body moves distance ΔL sequentially in the sliding direction of the



225 landslide, the corresponding time is recorded as $t_1, t_2, t_3 \dots t_n$, and the corresponding
226 velocity is expressed as $v_{x1}, v_{x2}, v_{x3} \dots v_{xn}$.

227 (4) The horizontal acceleration at t_0 can be calculated by Eq. (15) and is denoted
228 as a_{x0} , and the velocity at time t_0 is zero. After sliding distance ΔL is reached, the
229 following equations can be obtained.

$$230 \quad v_{x1} = \sqrt{2a_{x0}\Delta L} \quad (22)$$

$$231 \quad t_1 = t_0 + \sqrt{\frac{2\Delta L}{a_{x0}}} \quad (23)$$

232 (5) At $t=t_1$, the landslide body has horizontally moved by a distance ΔL in the
233 sliding direction of the landslide, zone 1 has slipped from the sliding surface. The
234 horizontal acceleration a_{x1} at t_1 is still calculated by Eq. (15). Unlike t_0 , the weight for
235 zone (n-1) changes to the weight for zone n, and the weight for zone (n-2) becomes the
236 weight for zone (n-1), and so on (at this time, there is no grid column for zone n). After
237 a_{x1} is calculated, the following can be established.

$$238 \quad v_{x2} = \sqrt{2a_{x1}\Delta L + v_{x1}^2} \quad (24)$$

$$239 \quad t_2 = t_1 + \frac{v_{x2} - v_{x1}}{a_{x1}} \quad (25)$$

240 (6) The calculation is continued in turn. When the obtained horizontal acceleration
241 is negative, the maximum velocity can be obtained. Finally, a_x and v_x in the calculation
242 process can be plotted as respective curves versus the sliding time.

243 2.7 Calculation of the waves height

244 The China Institute of Water Resources and Hydropower Research proposed an
245 empirical formula for waves height calculation (Zhong et al., 2007). In the formula, the
246 main factors that affect the waves height are the sliding velocity and volume of the
247 landslide. The formula for calculating the maximum waves height is as follows.

$$248 \quad \xi_{\max} = d \frac{v_m^{1.85}}{2g} V^{0.5} \quad (26)$$

249 where ξ_{\max} is the maximum waves height (m); d is the comprehensive influence
250 coefficient, with an average value of 0.12; v_m is the maximum sliding velocity (m/s); V
251 is the volume of the landslide body in the water (m³); and g is gravitational acceleration,
252 which equals 9.8 m/s².



253 The formula for calculating the waves height at different distances from the
 254 landslide body is as follows.

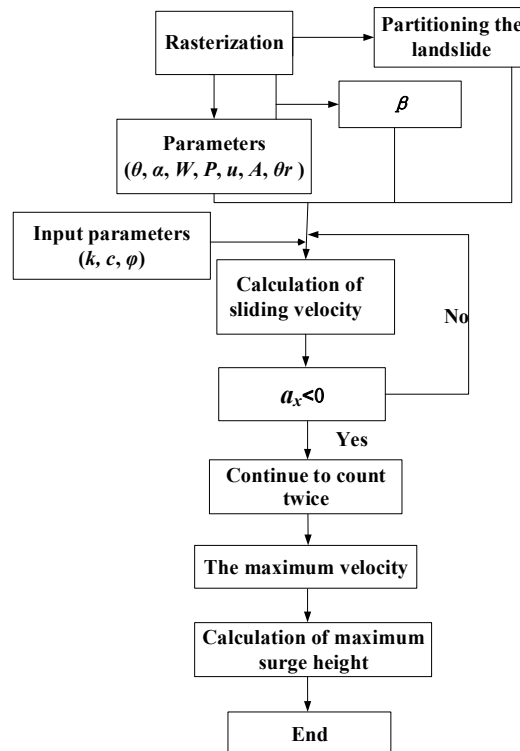
$$255 \quad \xi = d_1 \frac{v_m^n}{2g} V^{0.5} \quad (27)$$

256 where ξ is the waves height at a distance of L metres from the landslide body (m); n is
 257 the calculation coefficient, which is 1.4; and d_1 is the influence coefficient related to
 258 distance L , which is determined by the following formula.

$$259 \quad d_1 = \begin{cases} 0.5 & , (L \leq 35) \\ 6.1274L^{-0.5945} & , (L > 35) \end{cases} \quad (28)$$

260 3. Program implementation

261 Combined with the waves height calculation method, an expansion module was
 262 developed based on component object model (COM) technology in the ArcGIS
 263 environment. Fig. 7 illustrates the computational process.



264

265

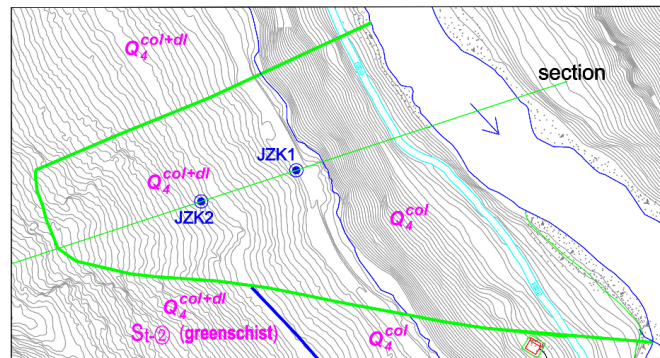
Fig. 7. The computational process.

266 4. Case study



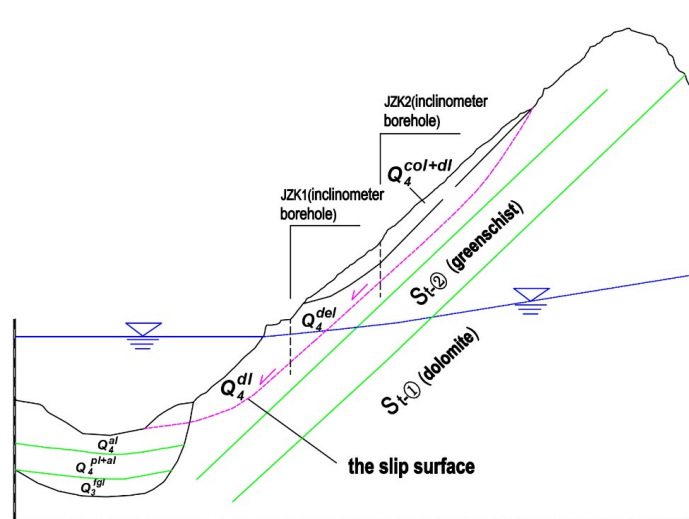
267 **4.1. Overview of the project**

268 The Kaiding landslide is approximately 14.5 km away from the dam of the
269 Houziyan hydropower station in Sichuan, China. The length of the landslide along the
270 river is approximately 490 m, the top elevation is 2080 m, the bottom elevation is 1754
271 m, and the volume is approximately 4.5 million cubic metres. Plan and section views
272 are shown in Fig. 8 and Fig. 9, respectively.



273
274

Fig.8. The plan view of the Kaiding landslide.



275
276

Fig. 9. The section view of the Kaiding landslide.

277 **4.2. Calculation of the sliding velocity**

278 The unit size of a grid column is 5 m×5 m, and $\Delta L = 10$ m. The internal friction
279 angle φ at the slip surface is 22.8° , the natural unit weight is 18.84 kN/m^3 , the buoyant
280 unit weight is 19.43 kN/m^3 , the buoyant density is $2.11 \times 10^6 \text{ g/m}^3$, and the elevation of
281 the reservoir water level is 1810.3 m. When the landslide body slides, the effective
282 cohesion c at the slip surface will decrease to 0, that is, $c=0$ (Pan, 1980). Using this



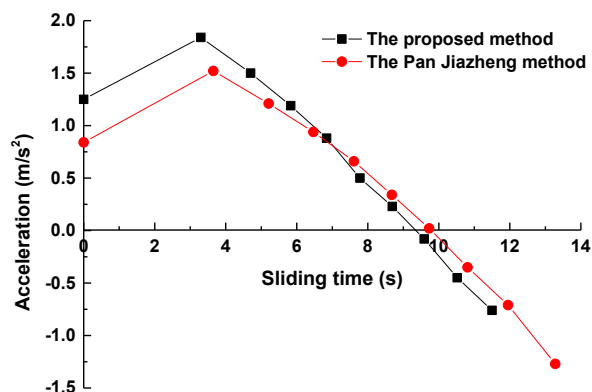
283 method and Pan Jiazheng's 2D method, the acceleration and velocity curves with the
 284 sliding time can be obtained, as shown in Fig. 10 and Fig. 11, respectively. The
 285 calculation results are shown in Table 1.

286 **Table 1** Calculation results

The Pan Jiazheng method			The proposed method		
t (s)	a_x (m/s ²)	v_x (m/s)	t (s)	a_x (m/s ²)	v_x (m/s)
0	0.84	0	0	1.25	0
3.65	1.52	5.48	3.30	1.84	6.07
5.21	1.21	7.35	4.70	1.50	8.17
6.47	0.94	8.49	5.83	1.19	9.52
7.61	0.66	9.17	6.84	0.88	10.40
8.68	0.34	9.49	7.78	0.60	10.96
9.73	0.02	9.51	8.67	0.28	11.21
10.81	-0.35	9.13	9.57	-0.08	11.14
11.95	-0.71	8.33	10.48	-0.45	10.73
13.28	-1.27	6.74	11.45	-0.90	9.86

287 The calculation results indicate that the maximum velocity obtained by the
 288 proposed method is 11.21 m/s, the starting acceleration is 1.25 m/s², and the sliding
 289 time required to reach the maximum velocity is 8.67 s. In comparison, the maximum
 290 velocity obtained by the Pan Jiazheng method is 9.51 m/s, the starting acceleration is
 291 0.84 m/s², and the sliding time required to reach the maximum velocity is 9.73 s.

292 Comparing the results of the proposed method with those of the Pan Jiazheng
 293 method, the maximum velocity of the proposed method is 15.2% higher than that
 294 calculated by the Pan Jiazheng method, the starting acceleration is 32.8% higher, and
 295 the sliding time required to reach the maximum velocity is 1.06 s short.



296
 297

Fig. 10. Horizontal acceleration curve with the sliding time.

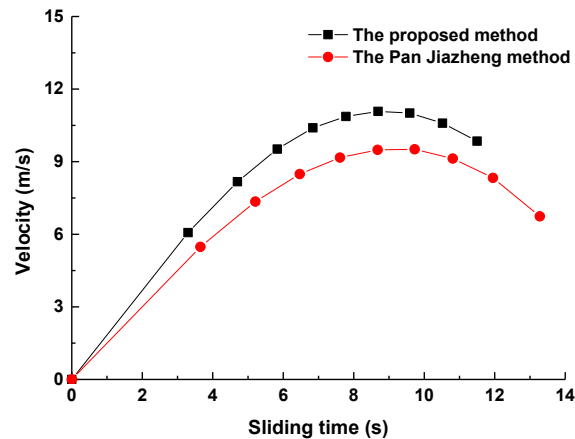


Fig. 11. Sliding velocity curve with the sliding time.

298
299

300 4.3. Waves analysis

301 According to the most dangerous working conditions, it is assumed that the
302 landslide body all slips into the water. The volume V of the landslide body under water
303 is $340 \times 10^4 \text{ m}^3$. According to Eqs. (26) and (27), the maximum waves height obtained
304 by the proposed method is 9.66 m, and the waves height at the dam site is 0.56 m. The
305 maximum waves height obtained by the Pan Jiazheng method is 7.28 m and the waves
306 height at the dam site is 0.44 m.

307 The landslide is approximately 14.5 km from the dam, the crest elevation is
308 1847.02 m, and the elevation of the reservoir water level is maintained at 1810.3 m.
309 When the waves height at the dam site is 0.56 m, water will not flow over the dam crest
310 and the safe operation of the dam will not be affected.

311 The maximum waves height obtained by the proposed method is 24.6% larger than
312 that based on the Pan Jiazheng method, and the waves height at the dam site obtained
313 by the proposed method is 21.4% larger than that based on the Pan Jiazheng method.

314 The calculations indicate that the results of the 2D method are smaller than those
315 of the 3D method. Compared that of the 2D method, the computational model of the
316 3D method better represents the actual spatial state of the landslide. As an analytical
317 method, the 3D model in this paper is more suitable than the 2D model.

318 5. Conclusions

319 Combined with the powerful spatial analysis ability of GIS, a 3D landslide force
320 analysis model based on grid column units was established. The dynamic equilibrium
321 equation for calculating the sliding velocity of a 3D landslide was derived to calculate



322 the waves height by combining Newton's laws of motion. To make the calculation more
323 convenient, an expansion module is developed to calculate the waves height in GIS,
324 and the feasibility of the module is verified by a case study.

325 Through calculations based on the case study, the maximum waves height
326 calculated by the 3D method proposed in this paper is 24.6% larger than that based on
327 the 2D Pan Jiazheng method, and the sliding time required to reach the maximum
328 velocity is shorter by 1.06 s. The calculations indicate that the results of the 2D method
329 are smaller than those of the 3D method.

330 Because the Pan Jiazheng method is based on a 2D section, the calculation results
331 will vary with the selected section. In this paper, the 3D landslide body model based on
332 grid column units is used to overcome the above shortcomings, and the calculation
333 model better represents the actual spatial state of the landslide body. Therefore, the
334 proposed method is more suitable for practical risk assessment.

335

336 **Data availability:** All data generated or analysed during this study are included in this
337 published article.

338

339 **Author contributions:** G.Y. and M.X. conceived of the presented idea. G.Y.
340 implemented the algorithm, and developed the theory. G.Y., M.X., and A.F. revised the
341 manuscript critically. G.Y. and L.B. finished the programming work. A.F. checked the
342 language.

343

344 **Competing interests:** The authors declare that they have no conflict of interest.

345

346 **Acknowledgment:** I would like to express my sincere gratitude to Prof. Mowen Xie,
347 Lei Bu, and Asim Farooq for their motivation and for providing me access to their
348 immense knowledge during this research work. This work was supported by the
349 National Natural Science Foundation of China [grant numbers 41372370].

350

351

352

353



354 **References**

- 355 Ataie-Ashtiani, B. and Nik-Khah, A.: Impulsive waves caused by subaerial landslides,
356 *Environmental Fluid Mechanics*, 8, 263-280, 2008.
- 357 Cui, P. and Zhu, X. H.: Surge generation in reservoirs by landslides triggered by the wenchuan
358 earthquake, *Journal of Earthquake and Tsunami*, 5, 461-474, 2011.
- 359 Chow, C. Y.: An introduction to computational fluid mechanics, John Wiley and Sons, Inc.,
360 New York, 1979.
- 361 Di, R. M. and Sammarco, P.: Analytical modeling of landslide-generated waves, *Journal of*
362 *Waterway, Port, Coastal, and Ocean Engineering*, 134, 53-60, 2008.
- 363 Hu, G. T.: *Landslide dynamics*, Geological Press, Beijing, 1995. (in Chinese)
- 364 Huang, J. L., Zhong, Z. H., and Zhang, M. F.: Sliding velocity analysis of reservoir bank
365 landslides based on the improved vertical slice method, *Journal of Mountain Science*, 30,
366 555-560, 2012. (in Chinese)
- 367 Jia, N., Yang, Z. H., Xie, M. W., Mitani, Y., and Tong, J. X.: GIS-based three-dimensional
368 slope stability analysis considering rainfall infiltration, *Bulletin of Engineering Geology*
369 *and the Environment*, 74, 919-931, 2015.
- 370 Miao, T. D., Liu, Z. Y., Niu, Y. H., and Ma, C. W.: A sliding block model for the runout
371 prediction of high-speed landslides, *Canadian Geotechnical Journal*, 38, 217-226, 2011.
- 372 Montagna, F., Bellotti, G., and Risio, M. D.: 3D numerical modeling of landslide-generated
373 tsunamis around a conical island, *Natural Hazards*, 58, 591-608, 2011.
- 374 Mergili, M., Marchesini, I., Rossi, M., Guzzetti, F., and Fellin, W.: Spatially distributed three-
375 dimensional slope stability modelling in a raster GIS, *Geomorphology*, 206, 178-195, 2014.
- 376 Noda, E.: Water waves generated by landslides, *Journal of the Waterways, Harbors and Coastal*
377 *Engineering Division*, 96, 835-855, 1970.
- 378 Pan, J. Z.: *Stability of construction against sliding and landslide analysis*, Water Conservancy
379 Press, Beijing, China, 1980. (in Chinese)
- 380 Silvia, B. and Marco, P.: Shallow water numerical model of the wave generated by the Vajont
381 landslide, *Environmental Modelling & Software*, 26, 406-418, 2011.
- 382 Xie, M., Esaki, T., Zhou, G., and Mitani, Y.: Geographic information systems-based three-
383 dimensional critical slope stability analysis and landslide hazard assessment, *Journal of*
384 *Geotechnical and Geoenvironmental Engineering*, 129, 1109-1118, 2003.
- 385 Xie, M., Esaki, T., and Zhou, G.: GIS-based 3D critical slope stability analysis and landslide
386 hazard assessment, *Journal of Geotechnical and Geoenvironmental Engineering*, ASCE, 129,
387 1109-1118, 2003.
- 388 Xie, M., Esaki, T., and Zhou, G.: GIS-Based Probabilistic Mapping of Landslide Hazard Using
389 a Three-Dimensional Deterministic Model, *Natural Hazards*, 33, 265-282, 2004.



- 390 Xie, M., Esaki, T., and Cai, M.: GIS-based implementation of three-dimensional limit
391 equilibrium approach of slope stability, *Journal of Geotechnical and Geoenvironmental*
392 *Engineering*, 132, 656-660, 2006.
- 393 Xie, M., Esaki, T., Qiu C., and Wang, C.: Geographical information system-based
394 computational implementation and application of spatial three dimensional slope stability
395 analysis, *Computers and Geotechnics*, 33, 260-274, 2006.
- 396 Xu, F., Yang, X., and Zhou, J.: Experimental study of the impact factors of natural dam failure
397 introduced by a landslide surge, *Environmental Earth Sciences*, 74, 4075-4087, 2015.
- 398 Zhong, D.H., An, N., and Li, M. C.: 3D dynamic simulation and analysis of slope instability of
399 reservoir banks, *Chinese Journal of Rock Mechanics and Engineering*, 26, 360-367, 2007.
400 (in Chinese)
- 401 Zhang, T.: Analysis on the landslide-generated waves of yalong river basin and its impact on
402 reservoir area, Master thesis, Department of Constructional Engineering, Tianjin University,
403 Tianjin, China, 2016. (in Chinese)